Adaptive optics with a programmable phase modulator: applications in the human eye

Pedro M. Prieto, Enrique J. Fernández, Silvestre Manzanera, Pablo Artal

Laboratorio de Optica, Universidad de Murcia, Edificio C, Campus de Espinardo, E-30071 Murcia, Spain
pegrito@um.es, enriquej@um.es, silmanro@um.es, pablo@um.es

Abstract: Adaptive optics for the human eye has two main applications: to obtain high-resolution images of the retina and to produce aberration-free retinal images to improve vision. Additionally, it can be used to modify the aberrations of the eye to perform experiments to study the visual function. We have developed an adaptive optics prototype by using a liquid crystal spatial light modulator (Hamamatsu Programmable Phase Modulator X8267). The performance of this device both as aberration generator and corrector has been evaluated. The system operated either with red (633nm) or infrared (780nm) illumination and used a real-time Hartmann-Shack wave-front sensor (25 Hz). The aberration generation capabilities of the modulator were checked by inducing different amounts of single Zernike terms. For a wide range of values, the aberration production process was found to be linear, with negligible cross-coupling between Zernike terms. Subsequently, the modulator was demonstrated to be able to correct the aberrations of an artificial eye in a single step. And finally, it was successfully operated in close-loop mode for aberration correction in living human eyes. Despite its slow temporal response, when compared to currently available deformable mirrors, this device presents advantages in terms of effective stroke and mode independence. Accordingly, the programmable phase modulator allows production and compensation of a wide range of aberrations, surpassing in this respect the performance of low-cost mirrors and standing comparison against more expensive devices.

© 2004 Optical Society of America

Ocis codes: (010.1080) Adaptive optics; (350.4600) Optical engineering; (330.4460) Ophthalmic optics; (330.5370) Physiological optics

References and links

1. R. K. Tyson, *Principles of Adaptive Optics* (Academic Press, New York, 1998).
2. G. D. Love, "Wave-front correction and production of Zernike modes with a liquid-crystal spatial light modulator," Appl. Opt. **36**, 1517–1524 (1997).
3. D. T. Miller, X. Hong, and L. N. Thibos, "Requirements for segmented spatial light modulators for diffraction-limited imaging through aberrated eyes," G.D. Love, ed. *Proceedings of the 2nd International Workshop on Adaptive Optics for Industry and Medicine*, 63-68 (World Scientific, Singapore, 1999).
4. A. W. Dreher, J. F. Bille and R. N. Weinreb, "Active optical depth resolution improvement of the laser tomographic scanner," Appl. Opt. **28**, 804-808 (1989).
5. P. Artal and R. Navarro, "High-resolution imaging of the living human fovea: measurement of the intercenter cone distance by speckle interferometry," Opt. Lett. **14**, 1098-1100 (1989).
6. J. Liang, D. R. Williams, and D. T. Miller, "Supernormal vision and high-resolution retinal imaging through adaptive optics," J. Opt. Soc. Am. A **14**, 2884-2892 (1997).
7. A. Roorda and D. R. Williams "The arrangement of the three cone classes in the living human eye," Nature **397**, 520-522 (1999).
8. L. N. Thibos and A. Bradley, "Use of liquid-crystal adaptive-optics to alter the refractive state of the eye," Optom. Vis. Sci. **74**, 7, 581-587 (1997).
9. F. Vargas-Martín, P. M. Prieto, and P.Artal, "Correction of the aberrations in the human eye with a liquid-crystal spatial light modulator: limits to performance," J. Opt. Soc. Am. A **15**, 2552-2562 (1998)
10. E. J. Fernández, I. Iglesias, and P.Artal, "Closed-loop adaptive optics in the human eye," Opt. Lett. **26**, 746-748 (2001).

#4629 - $15.00 US Received 17 June 2004; revised 4 August 2004; accepted 13 August 2004
(C) 2004 OSA

11. H. Hofer, L. Chen, G. Y. Yoon, B. Singer, Y. Yamauchi and D. R. Williams, "Improvement in retinal image quality with dynamic correction of the eye's aberrations," Opt. Express **8**, 631-643 (2001), http://www.opticsexpress.org/abstract.cfm?URI=OPEX-8-11-631.
12. F. H. Li, N. Mukohzaka, N. Yoshida, Y. Igasaki, H. Toyoda, T. Inoue, Y. Kobayashi, and T Hara. "Phase modulation characteristics analysis of optically-addressed parallel-aligned nematic liquid crystal phase-only spatial light modulator combined with a liquid crystal display," Opt. Rev. **5**, 174-178 (1998).
13. P. M. Prieto, E. J. Fernández, S. Manzanera, and P. Artal. "Adaptive Optics in the Human Eye with a Liquid Crystal Programmable Phase Modulator," Invest. Ophthalmol. Vis. Sci. **44**, ARVO E-Abstract 998 (2003), http://abstracts.iovs.org/cgi/content/abstract/44/5/998.
14. A. Awwal, B. Bauman, D. Gavel, S. S. Olivier, S. Jones, J. L. Hardy, T. Barnes, and J. S. Werner "Characterization and operation of a liquid crystal adaptive optics phoropter," Proc. Soc. Photo-Opt. Instrum. Eng. **5169**, 104-122 (2003).
15. J. Santamaría , P. Artal, and J.Bescós, "Determination of the point-spread function of the human eye using a hybrid optical-digital method," J Opt Soc Am A **4**, 1109-1114 (1987).
16. E. J. Fernández and P. Artal, "Membrane deformable mirror for adaptive optics: performance limits in visual optics," Opt. Express **11**, 1056-1069 (2003), http://www.opticsexpress.org/abstract.cfm?URI=OPEX-11-9-1056.
17. P. M. Prieto, F. Vargas-Martín, S. Goelz, and P. Artal, "Analysis of the performance of the Hartmann-Shack sensor in the human eye," J. Opt. Soc. Am. A **17**, 1388-1398 (2000).
18. C. Ftaclas, R. Basedow, A. Nonnenmacher, F. Weindling, D. Story, and E. Nelan, "Hubble Space Telescope fine-guidance-sensor transfer function and its impact on telescope alignment and guidance," Appl. Opt. **32**, 1696-1702 (1993).
19. N. Doble, G. Yoon, L. Chen, P. Bierden, B. Singer, S. Olivier, and D. R. Williams, "Use of a microelectro-mechanical mirror for adaptive optics in the human eye", Opt. Lett. **27**, 1537-1539 (2002).
20. B. A. E. Saleh and M. C. Teich, *Fundamentals of Photonics* (Wiley-Interscience, 1991).
21. H. Hofer, P. Artal, B. Singer, J. L. Aragón, and D. R. Williams, "Dynamics of the eye's wave aberration," J. Opt. Soc. Am. A **18**, 497-506 (2001).

1. Introduction

Deformable mirrors are the most common technology used for the active element in current Adaptive Optics (AO) systems [1]. Although they offer advantages in terms of speed and phase smoothness, they also have important drawbacks like a limited stroke, inability to reproduce steep phase changes, and in most cases a high price.

Liquid crystal phase modulators are an alternative to deformable mirrors for wavefront shaping or correction [2]. The main advantage of this technology is the capability for reproducing abrupt phase maps, which additionally allows the use of wrapped phase representations, greatly increasing the device effective stroke. Also, they share some advantageous features typical of liquid crystal devices (e.g., low drive voltage requirements as compared to deformable mirrors) and, furthermore, they can profit from the advances in liquid crystal manipulation gained in other technological fields, to produce low cost devices in the near future. Among their drawbacks, a low temporal response is the most important. In addition, low efficiency and artifacts due to diffraction have been traditionally pointed out as major problems in liquid crystal spatial light modulators. However, these problems have been greatly reduced with a new type of modulators, basically consisting of an optically driven continuous sheet of liquid crystal, which are not pixelated and, therefore, are claimed to be virtually free from diffraction effects. Finally, the dispersion properties of the liquid crystal and the phase wrapping limits the performance of these devices when using polychromatic light [3].

The current applications of Adaptive Optics (AO) are well beyond Astronomy, and in particular, ophthalmic AO is one of the most active areas. Both the correction and controlled manipulation of the eye's aberrations permit the recording of high resolution retinal images and performing new experiments in Vision research. In the early 90's, correction with a deformable mirror in the eye [4] and speckle interferometry [5] were the antecedents of today's ophthalmic AO. Later, static corrections of the ocular aberrations were demonstrated by using both deformable mirrors [6,7] and liquid crystal spatial light modulators [8,9]. More recently, real-time closed-loop AO in the eye has been also reported [10,11] using deformable mirrors.

#4629 - $15.00 US Received 17 June 2004; revised 4 August 2004; accepted 13 August 2004
(C) 2004 OSA

In this work, a continuous liquid crystal spatial light modulator was evaluated as the active element in an adaptive optics system for Visual Optics applications. The device is a Hamamatsu X8267 Programmable Phase Modulator. Its performance as wavefront generator was checked by producing different amounts of single Zernike terms of increasing order. The generation quality was studied both by measuring the wavefront shape and by experimentally recording the point spread function images. The device capability as wavefront corrector was first evaluated in an open-loop compensation for an artificial eye. Finally, the device was used in a close-loop mode to correct the aberrations of a real eye in real time.

2. Apparatus

The Hamamatsu X8267 Programmable Phase Modulator (PPM) consists of an optically-addressed liquid crystal spatial light modulator optically coupled to an intensity light modulator [12]. The former is composed of a continuous layer of parallel-aligned liquid crystal, a light blocking layer and a photoresistive layer sandwiched between transparent electrodes. When an image of the desired phase map is displayed in the intensity light modulator, the spatial distribution of light over the photoresistive material causes the voltage between the electrodes to locally change, varying the effective refractive index and, consequently, inducing the associated wavefront distortion. Both elements are coupled through an optical system that removes pixelation. Therefore, the PPM is theoretically free from the diffraction patterns associated to the pixel structure typical in electrically-addressed liquid crystal devices [2]. For this particular model (X8267), phase maps can be generated with XGA resolution (1024×768 pixels) over the 20×20 mm liquid crystal active area that correspond to the central 768×768 pixels. This represents an improvement with respect to former verisions of the device, working with VGA resolution (480×480 active pixels) [13,14]. The maximum optical path difference was around 1 wavelength for $\lambda \approx 750$ nm. Wrapped phase maps were displayed onto the PPM as images with the contrast manipulated to achieve the correct phase values for the wavelength in use. Phase wrapping was performed between $-\pi$ and π for the shortest wavelength used in the study (633 nm) and between -0.97π and 0.97π for the other wavelenth (780 nm), which was too long to allow a complete 2π range of phase generation.

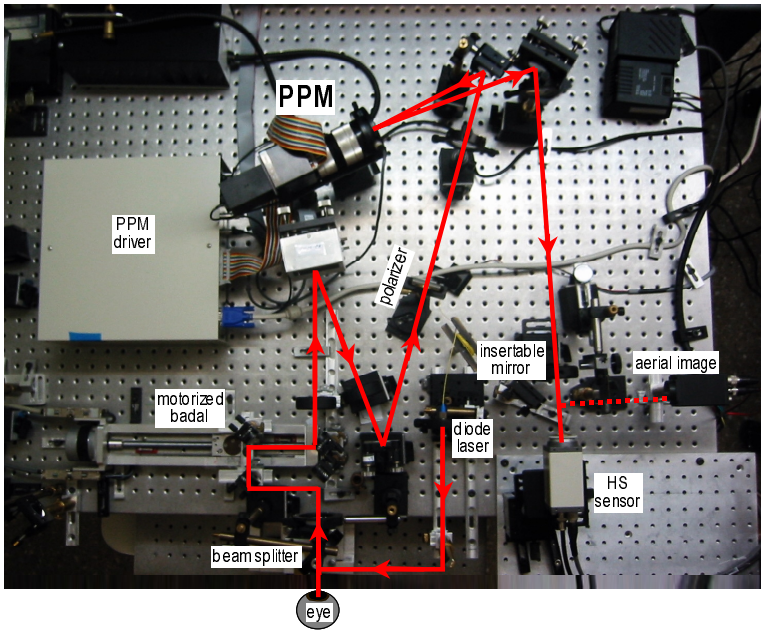

Fig. 1. Double-pass adaptive optics apparatus used to test the PPM.

#4629 - $15.00 US
Received 17 June 2004; revised 4 August 2004; accepted 13 August 2004
(C) 2004 OSA

The adaptive optics system (see Fig. 1) was based on a double-pass apparatus [15], previously used for AO applications in the eye [16]. The illumination channel used either a 633-nm He-Ne laser or a 780-nm diode laser as light source. The PPM was included in the measurement channel, which usually conveyed the light to the Hartmann-Shack (HS) sensor used for measuring the system aberrations [17], including those of the eye. Alternatively, double-pass (aerial) images were recorded by deflecting the light towards a CCD camera with a movable mirror that was inserted, when required, in front of the HS sensor (dashed line). In order to improve the pupil sampling in the PPM plane, a telescopic system was used to magnify the eye pupil plane by a factor of 2.5 onto the PPM plane. With this magnification value, a 5.5 mm eye pupil corresponds to 13.8 mm on the PPM. This value was convenient since it allowed displacements of the phase map over the PPM to fine tune alignment, while avoiding the use of areas of the PPM with poorer behavior (see Section 3).

A linear polarizer was inserted in the measurement channel since, by construction, the PPM requires the use of linearly polarized light. Additionally, a motorized focus-corrector system was included.

3. PPM calibration

The gain and the alignment of the PPM were first calibrated with the device inserted in the AO system. Additionally, the temporal response of the modulator was studied in order to determine the operation rate for close-loop correction in real eyes.

The voltage between the electrodes sandwiching the continuous liquid crystal layer depends on the gray level of the phase map image displayed onto the PPM. It is minimum for black and maximum for white. However, the induced phase depends on the illumination light wavelength both because of the relationship between optical path and phase, and because the dispersion properties of the liquid crystal. Accordingly, the PPM was calibrated to find the gain, α, between the gray level in the displayed phase map and the induced phase change. This calibration was performed by measuring changes in the polarization state introduced by different gray levels on a linearly polarized beam vibrating with 45º with respect to the liquid crystal optical axis.

The polarizer shown in Fig. 1 was rotated 45º and a second polarizer with the same axis was introduced after the PPM. This is termed by the manufacturer of the PPM as "intensity modulation mode" since changes in the induced phase map produce changes in the transmitted light. The camera for recording the aerial images was focused on the PPM surface and a collimated beam was used for illumination. The intensity distribution in the PPM plane (see Fig. 2-left) was recorded when flat images were displayed onto the PPM with different gray levels ranging from 0 (black) to 255 (white) in steps of 10. The set of intensity values was fitted to a sinusoidal function of the gray level, **g**,

$$I = I_1 + I_2 \cos[\alpha (\mathbf{g} - g_0)], \quad (1)$$

where the fitting parameters are I_1, the background intensity, I_2, half the polarized light intensity, g_0, the gray level origin, and α, is the required proportionality between gray level and induced phase. Only this latter parameter was of interest here since it is required to appropriately scale the phase maps to be displayed onto the PPM. The gray level origin, g_0, is unimportant since we are only interested in relative changes of phase in the wavefront. Furthermore, it can be controlled by setting a certain initial voltage between the electrodes sandwiching the liquid crystal layer. The intensity I_2 depends on the setup for the calibration. Finally, the background intensity, I_1, could be used to check the efficiency of the PPM but such a checking would require a much more precise measurement technique, which is beyond the scope of the present calibration procedure.

Provided that we have a series of images of the PPM surface, the fitting to Eq. (1) was performed locally in areas of 2×2 mm to average out the measurement noise. Fig. 2-right shows the set of local estimates of the gain, α. These values change toward one of the edges

#4629 - $15.00 US Received 17 June 2004; revised 4 August 2004; accepted 13 August 2004
(C) 2004 OSA

of the PPM, possibly due to differences in the thickness of the liquid crystal layer due to bending of the supporting sheets in the fabrication procedure. This problem, could be easily solved by using the local estimates of the gain. However, the current version of our control software does not allow the use of spatially varying gain. As a consequence, we opted for a smaller magnification between the pupil plane and the PPM to reduce the region in use to the central part (around 15x15 mm to allow fine-tuning in the position of the 13.8 mm pupil). Inside this area the PPM presents a more homogeneous behavior. Then, a single mean value of α was obtained by fitting using the mean intensity inside this area in the series of images. The calibration procedure was repeated for both of the wavelengths used in this experiment (see Fig. 3). For the red He-Ne laser (633nm) a mean value $\alpha = 0.0308$ was obtained, while for the near infra-red diode laser (780nm) the gain was $\alpha = 0.0238$. This latter value means a 1.93π range of phase generation for the PPM at 780 nm. As a consequence, phase wrapping could not be performed modulo 2π. This fact, however, did not produce noticeable effects inside the aberration range where the PPM correctly generated and compensated aberrations, presumably because of the small phase range not convered. Outside this range, part of the observed artifacts are probably attributable to this incomplete phase wrapping.

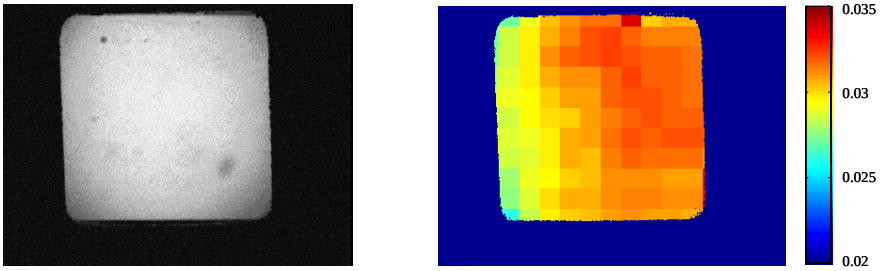

Fig. 2. Left panel: Intensity distribution on the PPM plane in intensity modulation mode when a flat image is displayed in the modulator for an illumination wavelength of 633nm. The bright square is the whole 20×20 mm active area of the PPM. Right panel: False color representation of the local estimates of the gain across the PPM surface for 633nm.

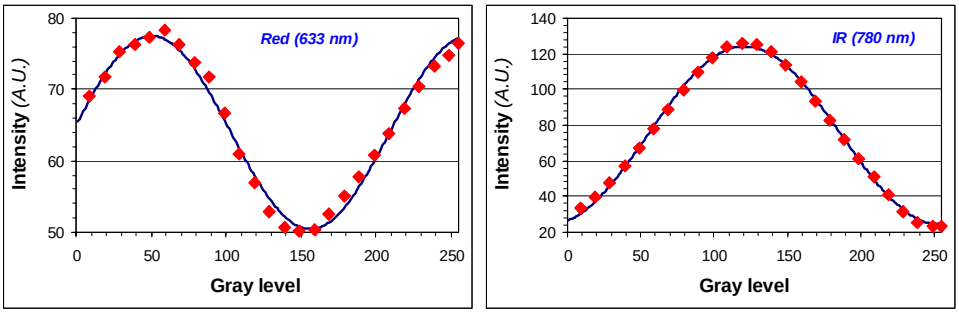

Fig. 3. Fitting to a sinusoidal function of the intensity in "intensity modulation mode" as a function of the gray level for red (left panel) and infrared light (right panel).

It is important to note that this calibration is performed with the PPM in place in the AO system and with minimal adaptations of other elements. A double advantage arises from this fact: on the one hand, the PPM gain is evaluated for the exact angle of incidence that will be used in the experiments; on the other hand, the calibration could be repeated for other wavelengths without dismantling the system.

A separate calibration procedure was devoted to check the alignment of the PPM in the AO system. Manipulation of the ocular aberrations requires precise alignment of the eye, the

#4629 - $15.00 US Received 17 June 2004; revised 4 August 2004; accepted 13 August 2004
(C) 2004 OSA

wavefront sensor and the active element. Properly setting this alignment is usually a time consuming task in the assembly of an AO apparatus. In our case, the phase map can be easily displaced in the PPM plane, and therefore alignment of this element is less critical and can be fine-tuned before each experimental run. To check the alignment, we directed a plane wavefront towards the PPM and measured the induced aberrations when a pure spherical aberration (Zernike term: n = 4, m = 0) was displayed onto the modulator. A misalignment of this kind of aberration is known to produce residual coma terms (n = 3, m = 1 for horizontal displacements, and n = 3, m = –1 for vertical displacements) [18]. Figure 4 shows the linear behavior of the coma terms when 0.63 μm (1 wavelength for the red illumination light) of spherical aberration is displaced in both horizontal and vertical directions. The displacements that produce 0 coma in each direction mark the pupil center position on the PPM plane with respect to the center of the active area of the modulator. With this procedure, the phase maps can be very precisely aligned with the eye's aberrations and the HS measurement area. However, considering the good linearity of the coma values, a faster method was used in practice: the spherical aberration phase map was digitally displaced both vertically and horizontally until the coma terms vanished. The pupil shifts experimentally found with this procedure were then used to displace the phase maps displayed through the experiment.

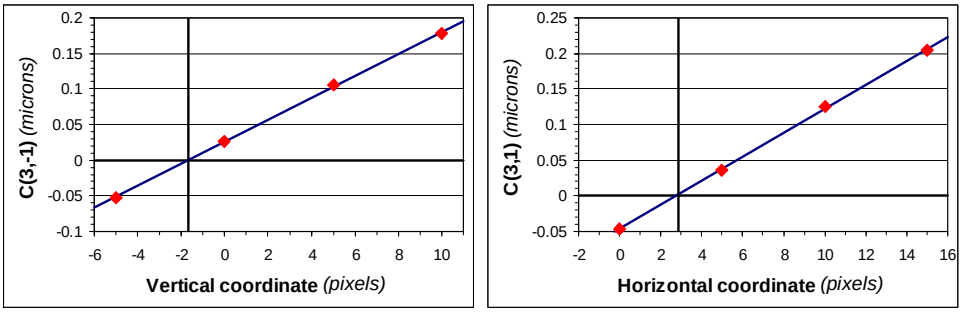

Fig. 4. Measured coma terms (red dots) generated by displacing a pure spherical aberration map across the PPM plane horizontally (left) and vertically (right) together with the respective linear fittings (blue lines). The bold lines show the displacements for 0 coma generation, which are used to precisely align the displayed phase maps with the AO system. The amount of spherical aberration was arbitrarily set to 0.63 μm.

Additionally, the magnification between the HS and the PPM planes was also experimentally controlled by generating a pure spherical aberration term. If the theoretical pupil size was not correct, a residual defocus appeared. Pupil size in the PPM plane was modified until the residual defocus was cancelled. In practice, the calibration of the alignment does not even require a plane wavefront to be directed towards the PPM: it is enough to compare the HS outputs for a constant and a spherical aberration phase maps displayed on the PPM. As a consequence, the complete procedure took just a few minutes to perform and was routinely repeated.

Finally, the temporal response of the device was studied. The apparatus was set in "intensity modulation mode" as described previously and we recorded the changes in the transmitted intensity when the PPM was switched between two constant (flat) images. These images were selected to produce a phase change close to π. Measurements were performed with a photodiode placed instead of the camera recording aerial images. The measuring rate was 1 kHz and the results are shown in Fig. 5. When the image switching is performed, the intensity changes as the liquid crystal molecules get oriented in an exponential-like behavior. The response time was evaluated as the time required to produce a 90% of the total intensity change. From Fig. 5, the response time of the PPM was found to be 0.26 sec. Accordingly, the update rate for the close-loop correction was set to approximately 4 Hz.

#4629 - $15.00 US Received 17 June 2004; revised 4 August 2004; accepted 13 August 2004
(C) 2004 OSA

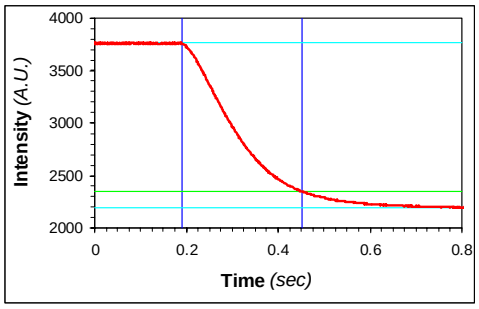

Fig. 5. Temporal response of the PPM when switched between two flat images. Red line: intensity transmitted in "intensity modulation mode"; cyan lines: asymptotic intensity transmitted for each image; green line: 90% of the phase shift; blue lines: times of image switch and 90% of phase change.

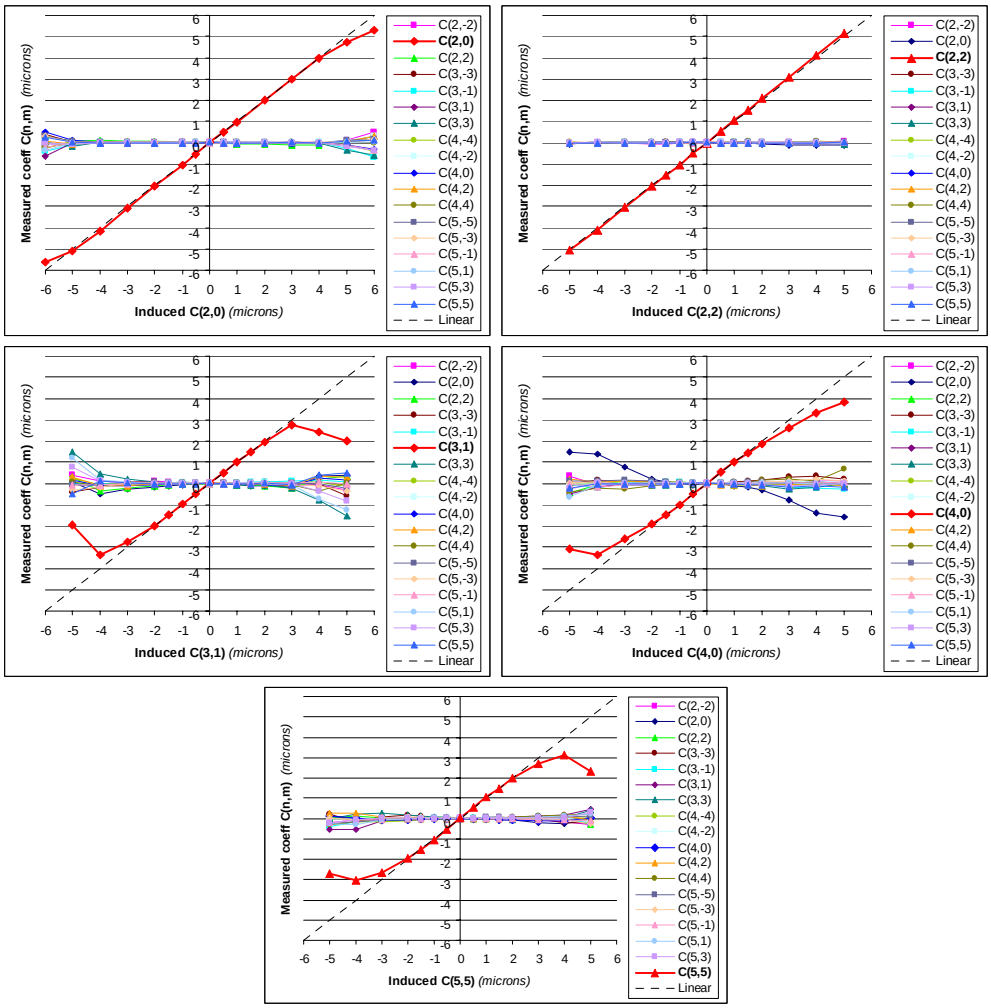

Fig. 6. Zernike terms measured with the HS sensor when inducing with the PPM different amounts of defocus (*C(2,0)*), astigmatism (*C(2,2)*), coma (*C(3,1)*), spherical aberration (*C(4,0)*) and pentafoil (*C(5,5)*). All the coefficients are expressed in microns over a 5.5 mm pupil in the eye pupil plane.

#4629 - $15.00 US
Received 17 June 2004; revised 4 August 2004; accepted 13 August 2004
(C) 2004 OSA

4. Performance of the PPM as an aberration generator

The performance of the PPM as a phase generator was evaluated by displaying different amounts of single Zernike modes into the modulator and then measuring the produced wavefront aberration with the HS sensor when using a 633-nm plane wavefront for illumination and considering a 5.5 mm pupil in the eye pupil plane. Additionally, aerial images were recorded to check for possible spurious artifacts in the phase manipulation procedure.

Figure 6 shows the measured coefficients (up to 5-th order) provided by the HS when the PPM was fed with increasing values of the following Zernike terms: defocus (n = 2, m = 0), cardinal astigmatism (n = 2, m = 2), horizontal coma (n = 3, m = 1), spherical aberration (n = 4, m = 0) and pentafoil (n = 5, m = 5). In all cases, an almost perfect correlation between the intended and the produced amount of the corresponding Zernike mode was found for a wide range of values, while negligible amounts of other terms were generated. For higher values, the linearity begins to fail and other terms start appearing in the measured wavefront. The coefficients are expressed in μm over a 5.5 mm pupil in the eye pupil plane.

Inside the linear range of the PPM, it reliably generates isolated aberration modes. By comparing these results with those found for other phase manipulating devices such as deformable mirrors [16,19], the PPM can deal with larger amounts of aberration than other low- or moderate-cost deformable mirrors.

Furthermore, it is important to note that the aberration generation process is not an iterative process as it is typically required when dealing with deformable mirrors. This is the case because of the poor fidelity and the non-linearity of the phase generation process for that kind of device. Instead, for single modes there is a very good resemblance between the phase map displayed onto the PPM and that experimentally produced, requiring no further steps of correction, and the phase generation process is virtually linear, as can be perceived from the absence of spurious modes in the linear range of coma production (see Fig. 6).

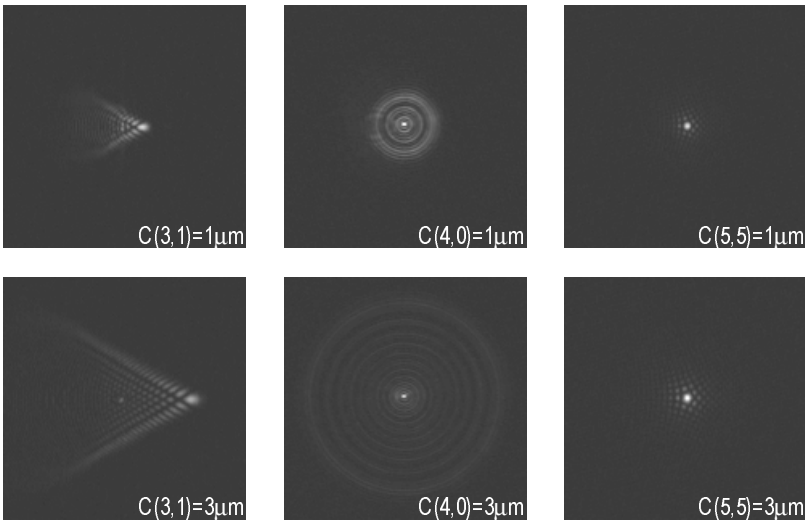

Fig. 7. Experimental aerial images for pure Zernike coma (*C(3,1)*), spherical aberration (*C(4,0)*) and pentafoil (*C(5,5)*). The upper panels correspond to 1 μm of the corresponding mode and the lower panels to 3 μm. The pupil size was 5.5 mm in all cases. A gamma correction (γ=2) has been introduced in every image to modify the contrast in order to make the faint fine structure apparent.

As a further test, we recorded the aerial images for the induced single Zernike values. Two of those images for coma, spherical aberration and pentafoil are shown in Fig. 7. For moderate values of each mode inside the linear range of aberration generation, the double-

#4629 - $15.00 US Received 17 June 2004; revised 4 August 2004; accepted 13 August 2004
(C) 2004 OSA

pass image resembles quite well the expected shape. For higher values, the shape is still easily recognizable but a spurious peak appears in the paraxial image position. This is particularly evident in the case of coma (lower-left) due to the asymmetry of the comatic point-spread function (PSF). This peak is assumed to be a 0-order diffractive artifact associated to the phase wrapping required by the PPM due to its limited phase stroke. The sources of this artifact may be residual pixelation effects, under-sampling problems in high phase slope areas, and/or failure to cover the whole 2π phase range. These diffraction problems might be reduced with a finer calibration or with a higher resolution device.

5. Aberration correction in an artificial eye

The AO system was used to correct the aberrations in an artificial eye. In this case, a diode laser (780nm) was used as light source. Fig. 8 presents the original wrapped aberration over a 5.5 mm pupil, the associated PSF and the experimentally recorded double-pass image. The initial root mean squared (RMS) of the wavefront was 0.518 μm and the associated Strehl ratio was 0.043. These images can be compared with those in Fig. 9, obtained with a single step correction, i.e., by displaying in the PPM the negative of the phase map in Fig. 8-left. The combined wavefront become virtually flat (RMS=0.067 μm). Consequently, the PSF collapses to a very narrow peak, which corresponds to a high Strehl ratio (0.749). This improves the resolution of the double pass images, although only the second pass is being corrected. The double-peak structure that appear in the compensated image corresponds to the propagation modes of the optical fiber used to couple the diode with the system [20]. When AO is off, it is blurred by the ocular aberrations to a single broad peak (Fig. 8, right panel). Successive correction steps further reduced the RMS (0.057 μm and 0.046 μm after the second and third iteration respectively) and increase the Strehl ratio (0.831 and 0.899), although visually the differences with the aerial image in Fig. 9-right are hardly apparent. This fine-tuning is probably due to the compensation of slight miscalibrations of the PPM (the local changes in the gain, the pupil size in the PPM plane, the pupil centering, etc.).

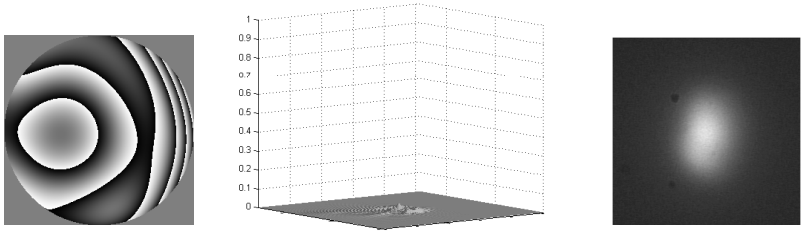

Fig. 8. Wavefront aberration map wrapped in the range [–0.97π, 0.97π] (left), associated PSF (center), and experimental aerial image (right) for the artificial eye with the adaptive optics OFF.

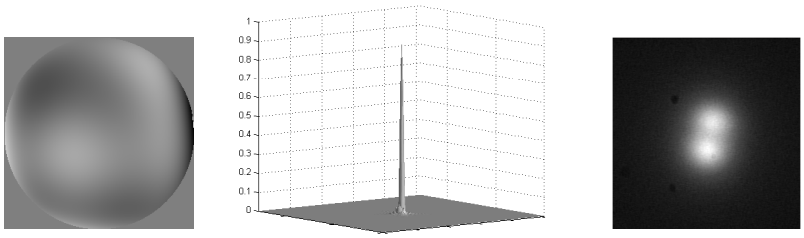

Fig. 9. Wavefront aberration map wrapped in the range [–0.97π, 0.97π] (left), associated PSF (center), and experimental aerial image (right) for the artificial eye with the adaptive optics ON after one single iteration (open-loop mode).

#4629 - $15.00 US Received 17 June 2004; revised 4 August 2004; accepted 13 August 2004
(C) 2004 OSA

This procedure corresponds to an open-loop correction. Open-loop operation requires a high fidelity between the wavefront sensor outcome and the phase map finally produced by the active element. Deformable mirrors typically present non-linearities that force close-loop operation [16]. On the contrary, these results shows the capability of the PPM to work open-loop or even in a single step.

6. Closed-loop aberration correction in a real eye

As a final step of our testing of the performance of the PPM for Visual Optics applications, we performed a closed-loop correction in real eyes. We modified our real-time (25 Hz) HS wavefront sensor control software in order to feed the PPM with the instantaneously measured aberrations. Due to the slow response of the modulator (around 1/4 sec.), the loop was slowed to work around 4 Hz. Correction was performed on five normal subjects (JB, JF, PA, PP, SM) with unparalyzed accommodation and undilated pupil. The pupil diameter was artificially set to 5.5 mm on the subject's pupil plane. Although no careful best-focus search was performed, the defocus term was reduced before each experiment with the aid of the motorized focus corrector for the ammetropic subjects (JB, PA, and PP). After this, the defocus term is treated as any other aberration term and corrected with the PPM. The RMS values provided include this defocus term.

Although the PPM reproduces the intended phase map with a high fidelity, the process is too slow to follow the ocular aberration dynamics, which have been shown to have relevant spectral components up to 5Hz [21]. As a consequence, closed-loop correction tended to become unstable unless an attenuation factor, or gain, between the measured aberration and the displayed phase map was introduced. Figure 10 shows the effect of this parameter in the closed-loop behavior for one of the subjects (JB). We have represented the evolution of the RMS of the eye's aberrations, including astigmatism and residual defocus at best focus, during correction. In all the cases, the RMS is reduced from around 1.7 μm, with an important astigmatism component, to values around 0.1 μm. However, as it was to be expected, low values of attenuation increase the convergence time, although they produce a smoother behavior. As a compromise between these two effects we selected a value of 0.3 for the attenuation factor as our standard.

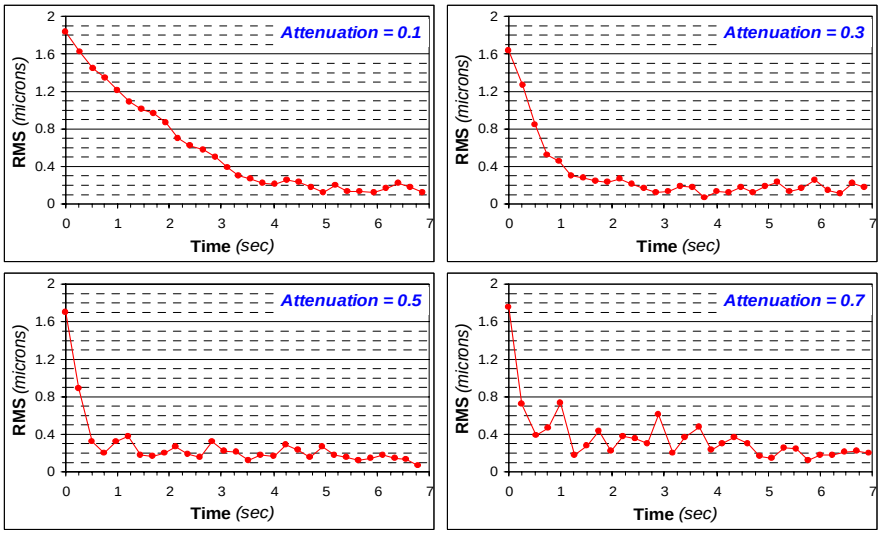

Fig. 10. Temporal evolution of the RMS of subject JB during close-loop corrections of the ocular aberrations with the PPM for different values of the close-loop attenuation.

#4629 - $15.00 US Received 17 June 2004; revised 4 August 2004; accepted 13 August 2004
(C) 2004 OSA

It has to be pointed out that this attenuation is the ultimate responsible of the gradual behavior of the RMS in Fig. 10 (and later in Fig. 11) at the beginning of the loop, while the asymptotic value of around 0.1 μm and the instabilities in the RMS are attributed to the ocular aberration dynamic components faster than the aberration rate. For a static artificial eye, where no attenuation is required, correction from Fig. 8 to Fig. 9 is achieved in around ¼ sec and the correction level remains virtually constant after that point.

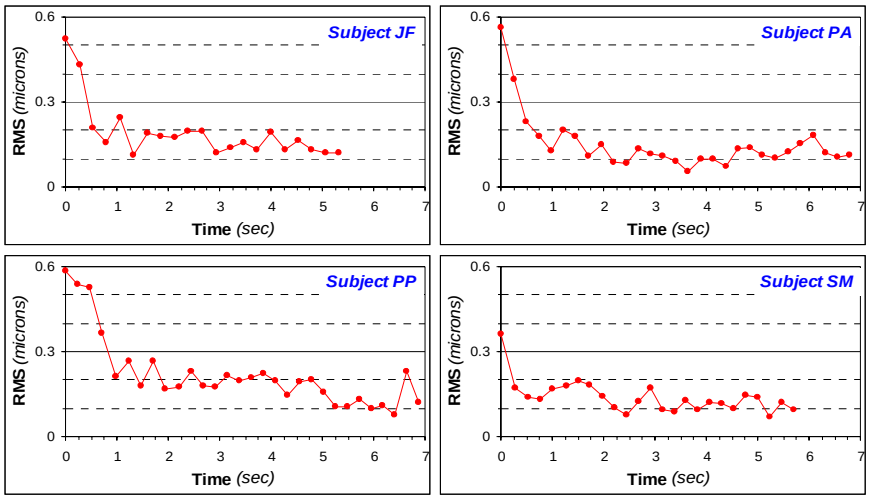

Fig. 11. Temporal evolution of the RMS of subject JF, PA, PP, and SM during close-loop corrections of the ocular aberrations with the PPM for a close-loop attenuation of 0.3.

In Fig. 11, we represent the temporal behavior of the RMS during correction for the other subjects studied. The initial RMS was lower than for subject JB but values around 0.1 μm were consistently obtained in 4 iterations, corresponding to 1 sec of closed-loop operation.

Form Figs. 10 and 11, it can be appreciated that a closed-loop operation of the PPM effectively improves the eye's optical quality. The reduction in the RMS increases the image quality of the corrected eye. This fact is apparent in Fig. 12, where the initial aberration map and PSF for each subject can be compared with those after 3 sec of AO correction, selected as examples of the results obtained after a few steps of correction.

To quantify the improvement, table 1 shows the initial values of RMS and Strehl for each subject together with the mean corrected values associated to the AO correction calculated by average after discarding the first 2 seconds of the experiment. For the attenuation factor considered, this delay is theoretically wide enough for the AO system to reach the asymptotic correction regime. For comparison purposes, Table 1 also shows the best Strehl in each experiment and the corresponding RMS.

Table 1. RMS and Strehl ratio associated to the AO correction for each subject. The initial values are those found for the uncorrected eye. The mean corrected values correspond to the asymptotic average obtained by discarding the first 2 seconds of each series. The best values are the higher Strehl and the associated RMS in the series.

Subject	Initial vlues		Mean corrected (after 2 sec)		Best value in the experiment	
	RMS	Strehl	RMS	Strehl	RMS	Strehl
JB	1.636	0.012	0.168	0.353	0.069	0.763
JF	0.525	0.040	0.152	0.343	0.120	0.534
PA	0.562	0.027	0.112	0.515	0.056	0.840
PP	0.587	0.037	0.166	0.322	0.076	0.738
SM	0.363	0.109	0.111	0.536	0.071	0.767

#4629 - $15.00 US Received 17 June 2004; revised 4 August 2004; accepted 13 August 2004
(C) 2004 OSA

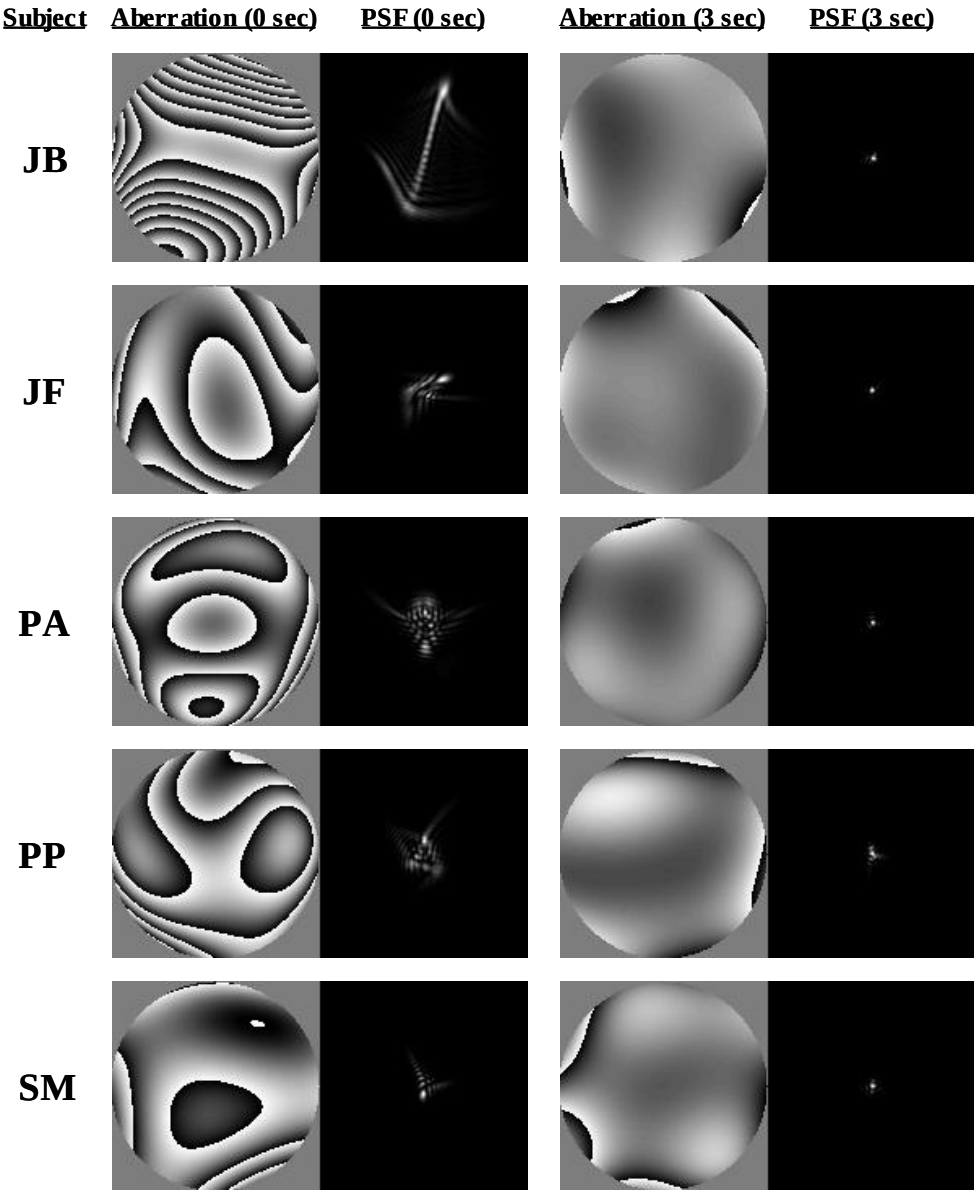

Fig. 12. Aberration maps and PSFs at the beginning of close-loop AO correction and after 3 sec. of operation. The associated wavefront RMS and the Strehl ratio for each PSF can be found in table 1. The images correspond to the series displayed in Fig. 10 (attenuation = 0.3) for subject JB and Fig. 11 for the rest of the subjects.

As a final demonstration of the correction process, Fig. 13 shows in a multimedia file the phase maps and the associated PSFs for subject JB during AO correction with the PPM. To provide with an idea of the speed of the process, the video rate has been set to 4 Hz. Each PSF image has been scaled to its maximum intensity. The aberration map can be seen to become flat rapidly, with most of the 2π phase jumps removed in 4 frames (around 1 sec.). Accordingly, the PSF collapses from the shape associated to the subject's aberrations, dominated by the astigmatism, to a narrow peak.

#4629 - $15.00 US Received 17 June 2004; revised 4 August 2004; accepted 13 August 2004
(C) 2004 OSA

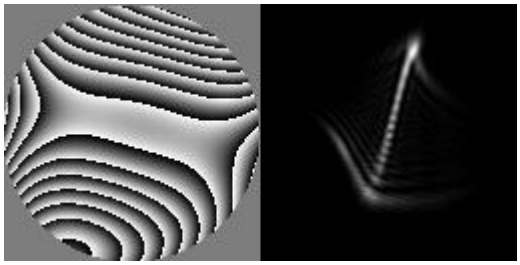

Fig. 13. Multimedia file (2.81 Mb) showing the evolution of the wavefront map and the associated PSF during a close-loop AO correction on subject JB using the PPM. The video rate is set to 4 Hz to approximately match the PPM operation rate. Each individual PSF is normalized to its maximum.

7. Conclusions

In this study, a Programmable Phase Modulator (X8267 from Hamamatsu) was tested as the active element of an adaptive optics system for Visual Optics applications, both as wavefront generator and corrector. The capacity of working with wrapped phase maps greatly increases the PPM effective stroke. The range of linear production of aberrations is larger than those typical in most deformable mirrors. Besides there is virtually no cross-coupling inside this linear range. The PPM was tested as wavefront corrector in an artificial eye, reducing its aberrations to a negligible value in a single step. The high fidelity of the device for reproducing the intended phase map allows open-loop operation, typically impracticable with deformable mirrors. Finally, a closed-loop correction was performed in a real eye. The slow temporal response of the modulator, which is probably its major drawback, imposed a reduction on the aberration display rate to a value around 4 Hz. This update frequency is a little below the highest frequency of the relevant components of the ocular wavefront dynamics. As a consequence, the residual RMS after correction was higher than for the artificial eye case and the instability appeared in the correction loop. The latter effect was reduced by including a gain in the close loop, although this increased the convergence time. Another potential problem are diffraction effects. The sources of this artifact may be residual pixelation effects, under-sampling problems in high phase slope areas, and/or failure to cover the whole 2π phase range. These diffraction problems might be reduced with a better calibration of the system or with a higher resolution device. Nevertheless, the PPM proved to be capable of working as the active element in a close-loop adaptive optics system for the eye with an efficiency at least comparable to that achieved with low cost deformable mirrors.

Acknowledgments

This work was supported by the *"Ministerio de Ciencia y Tecnología"*, Spain, grant BFM2001-0391 to PA. The authors thank the help of José Salort with the control software development.

#4629 - $15.00 US Received 17 June 2004; revised 4 August 2004; accepted 13 August 2004
(C) 2004 OSA